PERGAMON

Journal of Structural Geology 23 (2001) 1179–1185

JOURNAL OF STRUCTURAL GEOLOGY

www.elsevier.nl/locate/jstrugeo

Centrifuge modelling of the evolution of low-angle detachment faults from high-angle normal faults

Hemin A. Koyi*, Alasdair Skelton

Hans Ramberg Tectonic Laboratory, Department of Earth Sciences, Uppsala University, Uppsala, Sweden

Received 4 May 2000; accepted 21 November 2000

Abstract

Centrifuge models composed of a ductile layer overlain by a semi-brittle layer are used to study how deformation localised by a high-angle normal fault promotes detachment faulting. During lateral extension driven by centrifugal force, localised extension along a pre-existing fault initiated localised isostatic upwelling of the denser lower layer. Where the lower ductile layer was significantly less dense than the semi-brittle upper layer, localised extension along the prescribed cut initiated upwelling of the ductile lower layer. Based on model results, we argue that the transition from high-angle normal faulting to low-angle 'detachment' faulting is an inevitable consequence of localising extension, provided that there is viscous coupling between the extending upper layer and the upwelling lower layer. In models with a lower layer of equal density or a denser lower layer, this rotation takes place at the later stages of localised thinning in the upper semi-brittle layer, whereas in models with a less dense lower layer, the rotation takes place earlier due to the buoyant rise of the ductile lower layer.

In areas of distributed crustal stretching (e.g. rift basins), where extension of the upper layer is accommodated by numerous steep faults distributed over a wide area and upwelling of lower ductile materials is 'distributed' across the area, normal faults remain more planar despite a large amount of extension. Models show that distributed extension along several closely spaced normal faults encourages rotation of blocks rather than their distortion to form listric faults. We further conclude that the only configuration whereby localisation of extension would not result in detachment-style faulting is when the upper and lower layers were completely decoupled.

Keywords: Extension; Low-angle detachment; OCT (Ocean-continent transition zone); Centrifuge models

1. Introduction

Detachment faults are low-angle normal faults. They are typically associated with (1) exhumation of the lower crust or even the mantle, normally enabled by (2) large lateral displacements. Detachment faults are reported in North America, Greece and China (Davis et al., 1980; Wernicke, 1981; Miller et al., 1983; Bartley and Wernicke, 1984; Selverstone, 1988; Lister and Davis, 1989; Lister et al., 1991, Burchfiel et al., 1992, Den Driessche and Brun, 1992; Axen et al., 1999 and the references therein), where they have exhumed high-grade lower crustal rocks. These *core complexes* are characterised by structural juxtaposition of (overlying) brittly-deformed low-grade upper crustal rocks and (underlying) lower crustal rocks. Detachment faults are further reported from both ancient and modern ocean–continent transition (OCT) zones, where they have exhumed mantle rocks. These *mantle windows* are characterised by structural juxtaposition of (overlying) brittly-deformed continental material and (underlying) ductily-deformed, highly serpentinised mantle material.

Despite playing a key part in both collisional and extensional tectonics, the mechanism whereby detachment faults exhume core complexes in orogenic belts and the mantle in some OCT zones remains poorly understood.

Three main models have been suggested for the origin of detachment faults: (1) the simple shear model (Wernicke, 1981, 1985), which assumes that detachment faults originate as low-angle (dip $< 30°$) normal faults, (2) the tilted block model (Angelier and Colletta, 1983; Davis, 1983), which assumes that steep normal faults separating large-scale blocks rotate to low-angle dips, and (3) the rotated normal fault(s) model (Buck, 1988; Wernicke and Axen, 1988) which assumes that detachment faults evolve from sequential development of high-angle normal faults. Brun et al. (1994) argued against the simple-shear model since initiation of faults at low angles is not supported by the Mohr–Coulomb theory of faulting or the study of focal mechanism of major earthquakes in extending areas.

Brun et al. (1994) used analogue models of brittle–ductile

* Corresponding author.
E-mail address: hemin.koyi@geo.uu.se (H.A. Koyi).

0191-8141/01/$ - see front matter
PII: S0191-8141(00)00185-1

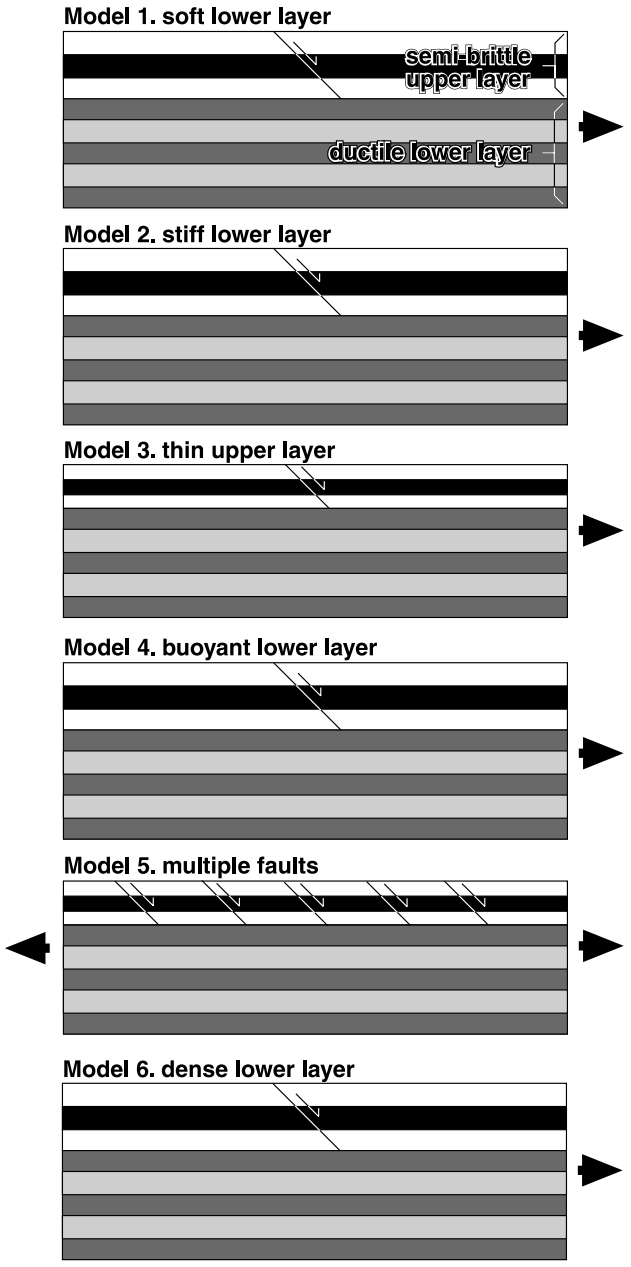

Fig. 1. Schematic line drawings of the initial set-up of models 1–6 showing the variable parameter in each model. For specifics of viscosity, density and thickness, see Table 1. Black arrows show extension direction. Half arrows show direction of movement along prescribed cuts.

layers to show that both of these processes act simultaneously in the formation of detachment faults and that detachment faulting is localised above a low-viscosity heterogeneity. Here, we present the results of a series of scaled centrifuge models to simulate the mechanism responsible for the formation of low-angle detachment faults from high-angle normal faults. In these models, three variables (thickness of the brittle layer, and density and viscosity of the ductile lower layer) were systematically changed to study their influence on the evolution of detachment faults.

2. Model preparation, kinematics and scaling

Six models with similar initial configuration were deformed in the centrifuge to study the mechanism responsible for the initiation of low-angle detachment faults (Fig. 1). Each model consisted of a ductile lower layer overlain by a semi-brittle layer. The ductile lower layer was prepared by mixing plastilina with a non-Newtonian viscous silicon polymer. The upper layer on the other hand, which was prepared by mixing plastilina with sugar powder, deformed in a semi-brittle manner that accommodated extension by faulting rather than flow during centrifuging. The upper layer had a constant density in all the six models, whereas the lower layer had a constant density of $1.56\ g\ cm^{-3}$ in all but two models (density was $1.24\ g\ cm^{-3}$ in model 4 and $1.61\ g\ cm^{-3}$ in model 6) (Table 1). In models 1–3 and 5, the density of the upper layer was identical to that of the lower layer. The reason for this was to accommodate the crust–mantle analogue. The average density of the crust ranges from $\sim 2.7\ g\ cm^{-3}$ (continental) to $\sim 3.0\ g\ cm^{-3}$ (oceanic). The average density of the uppermost part of the mantle ranges from $\sim 2.55\ g\ cm^{-3}$ to $3.3\ g\ cm^{-3}$ depending on the degree of serpentinisation. Because the degree of serpentinisation was not known, equal densities were chosen for both layers in four of the models (models 1–3, and 5) as the default case. In model 6, however, a denser lower layer (density $= 1.61\ g\ cm^{-3}$) and in model 4, a less dense lower layer (density $= 1.24\ g\ cm^{-3}$) was used in order to study the effect of density on the mode of deformation.

The effective viscosity of the lower layer was changed between stiff (10^6 Pa s) and soft (10^4 Pa s) (Fig. 2 and Table 1). Keeping the other parameters constant, in model 3, the thickness of the semi-brittle upper layer was decreased to 0.6 cm (compared with 1.2 cm in models 1, 2, 4 and 6) to study the influence of thickness variation on the deformation of the model. Mechanical properties and model variables and set-up are shown in Tables 1 and 2.

One prescribed cut was made in the upper semi-brittle layer of models 1–4 and model 6 at an arbitrarily chosen angle of 45° (Fig. 1). The surface of this cut was lubricated to ease movement before the blocks were put together. In order to study the effect of distributed extension on the mode of deformation, several prescribed cuts were made in the upper semi-brittle layer in model 5. In order to achieve extension, the models were allowed to collapse laterally in one direction during centrifuging. Only model 5, which contained five prescribed cuts in the semi-brittle upper layer, was allowed to extend in two opposite directions during centrifuging to avoid artificial localisation of deformation adjacent to a fixed wall. The amount of extension was controlled using spacers to limit the lateral extension of the models (Fig. 2). During extension in the centrifuge, the lower ductile layer spread laterally and initiated displacement along the prescribed cut in the upper layer (Fig. 3). The models were extended in stages.

Table 1
Material description and model parameters. (Densities are in g cm^{-3}, h_{ul} and h_{ll} represent the thickness of the upper and lower layers, respectively.)

Model	Lower layer			Upper layer		h_{ul}/h_{ll}	Final extension (%)	Result
	Material mixture	Viscosity	Density	Material mixture	Density			
1	Silicone, plastilina, acid oil and barite	Low	1.56	Plastilina, sugar powder and barite	1.56	0.6	28	Detachment faulting
2	Silicone, plastilina, acid oil and barite	High	1.56	Plastilina, sugar powder and barite	1.56	0.6	29	Detachment faulting
3	Silicone, plastilina, acid oil and barite	Low	1.56	Plastilina, sugar powder and barite	1.56	0.3	12.5	Detachment faulting
4	Dow Corning silicone and barite	High	1.24	Plastilina, sugar powder and barite	1.56	0.6	28	Detachment faulting
5	Silicone, plastilina, acid oil and barite	High	1.56	Plastilina, sugar powder and barite	1.56	0.6	52	No detachment faulting
6	Silicone, plastilina, acid oil and barite	High	1.61	Plastilina, sugar powder and barite	1.56	0.6	29	Detachment faulting

After each stage, the top of the model was photographed and vertical sections were cut for photographing. The section was then replaced and welded by contact. Models 1, 2, 4 and 6 were extended by about 30%, model 3 by 13% and model 5 was extended by 52% during centrifuging at $700 \times g$ (Table 1). All models were stopped when extension resulted in total separation of the two blocks (hanging wall and footwall) of the semi-brittle layer.

The dimensions of the models may be scaled to a natural prototype where 1 mm represents 1 km in models 1, 2, 4 and 6 and 1 mm represents 2 km in models 3 and 5 making the upper-layer thickness equal to 12 km. The scaling ratios of other parameters (e.g. density, stress, time and viscosity) are shown in Table 2. For scaling purposes (see Table 2) and to shorten the deformation time in the models, which consisted of materials that did not flow under normal gravity, models were deformed in a centrifuge. For details of the centrifuge technique and scaling, readers are referred to Ramberg (1981); Dixon and Summers (1985) and Koyi (1988, 1991).

3. Model results

During extension of all models, the pre-existing *faults* were activated. Extension in the semi-brittle layer was accommodated by movement along the fault, whereas the underlying layer accommodated extension by penetrative flow and upwelling locally, where the upper layer was progressively thinned by displacement along the *fault* (Fig. 3). A rollover anticline formed in the hanging wall block (Fig. 3). This structure amplified with increasing bulk extension until the two blocks separated. With continued extension and upwelling of the underlying layer, the two blocks separated and the ductile layer isostatically flowed upwards and filled the gap between them. This flow bent the footwall block upwards resulting in bending of the fault to become listric, shallowing to sub-horizontal towards the graben (Fig. 3). This deformation sequence was repeated in all six (1–6) models irrespective of the thickness of the brittle layer or the density or viscosity of the underlying ductile layer. In models 1–3 and 6, on the hanging wall

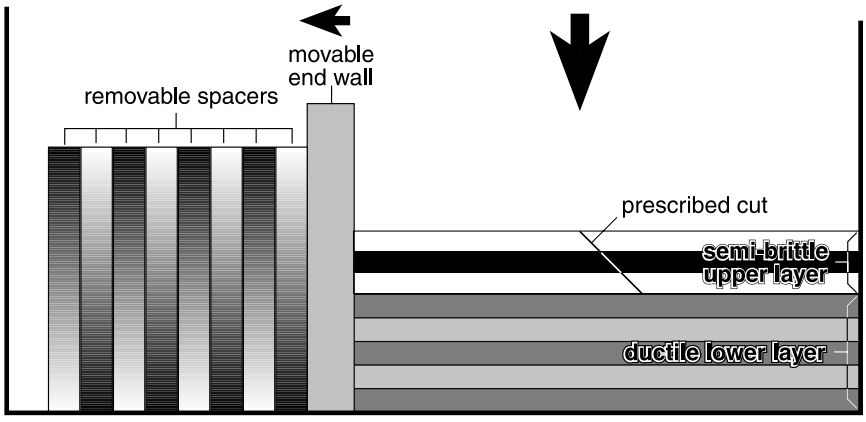

Fig. 2. Schematic diagram of the model set-up. Vertical arrow represents the centrifugal force.

Table 2
Scaling parameters between models and prototype. (Subscripts m and n denote model and prototype, respectively.)

Quantity	Nature	Model	Scaling ratio
Length ratio			
Upper layer	12 km	12 mm	$l_r = 1 \times 10^{-6}$
Lower layer	20 km	20 mm	$l_r = 1 \times 10^{-6}$
Density (kg m^{-3})			
Upper layer	2550	1560	$\rho_m/\rho_n = 0.6$
Lower layer	2300–2550	1100–1550	$\rho_m/\rho_n = 0.5$
Acceleration	1	700	$a_r = 700$
Stress ratio			$\sigma_r = a_r l_r \rho_r = 3.5$–$4.2 \times 10^{-4}$
Velocity (mm yr^{-1})	5–20[a]	1.3×10^6	$V_r = 6.5 \times 10^4$–2.6×10^5
Time	0.17–0.67 my[b]	810 s	$t_r = l_r/v_r = 3.8 \times 10^{-11}$–$1.5 \times 10^{-10}$
	1.7–6.7 my[c]		$t_r = l_r/v_r = 3.8 \times 10^{-12}$–$1.5 \times 10^{-11}$
	1.9–49.5 my[d]		$t_r = l_r/v_r = 5.2 \times 10^{-13}$–$1.3 \times 10^{-11}$
Viscosity (Pa s)	1.1×10^{19}–3×10^{21}[c]	$5 \times 10^{4-6}$	$\mu_r = \sigma_r t_r = 1.6$–$4.5 \times 10^{-15}$

[a] From Sawyer (1994) and Harry and Bowling (1999).
[b] Calculated from model parameters for a 1.2 km upper layer.
[c] Calculated from model parameters for a 12 km upper layer.
[d] Calculated from model parameters for a 24 km upper layer.

side, however, the fault became anti-listric due to the rollover of the hanging wall block adjacent to the fault. In model 5, where deformation was mainly by rotation of the semi-brittle blocks with insignificant internal deformation of the individual blocks, the rise of the ductile layer was more distributed than the other models.

4. Discussion

The transition from high-angle normal faulting to low-angle detachment faulting is critical to our understanding of the tectonic exhumation of: (1) core complexes in extensional domains, and (2) mantle material at both present day and fossil non-volcanic ocean–continent transitions.

Results of our models show that density and viscosity of the lower layer and thickness of the crust is mostly irrelevant to the formation of detachment faults. The lower layer rises to fill the space created between separated crustal blocks, irrespective of its density and viscosity (Fig. 3). Less dense lower layer material (as in model 4) will rise buoyantly, whereas equal density and more dense mantle material (as in models 1–3, and 6) will rise due to isostacy. Upward bending of the lower layer as a regional isostatic response to normal fault motion is portrayed in the numerical models of Buck (1988) and Buck et al. (1988). Based on field observations, Wernicke and Axen (1988) argued that profound, isostatically driven deformation of the footwalls of major normal faults may be common in extensional terrains. In all the models presented here, the upwelling of the lower layer is accompanied by viscous drag along the base of the footwall and rotation of the *fault* to low angle. As a result, the pre-existing high-angle normal fault rotates to a sub-horizontal detachment fault. The models also show that, even in the absence of a *weak heterogeneity* zone (Brun et al., 1994) in the mantle, homogeneous lower layer material wells upwards due to isostacy beneath the thinning crust and then fills the gap between the two separating crustal blocks.

The flow of the ductile lower layer during extension of the model is slightly asymmetric. Considering a simple shear mode of extension due to the presence of the prescribed cut in the upper layer, the upwelling of the lower layer is *surprisingly* symmetrical (the asymmetry is very small). In the model with a stiff lower layer, however, this asymmetry is more profound. This slight asymmetry is also shown in the numerical models by Boutilier and Keen (1994). In general, however, even though the doming of the lower layer is not profoundly asymmetrical, the internal flow of the lower material is clearly asymmetric (Fig. 3). This asymmetry is due to the difference in deformation mechanism of the hanging wall and footwall along the prescribed cut. During extension, the hanging wall subsides into the underlying ductile layer, whereas the footwall is locally uplifted (Fig. 3).

The models described here are deformed in a centrifuge at $700 \times g$ for 810 s (Table 2). Scaled to nature, this model-deformation time corresponds to 1.7–6.7 Ma depending on velocity and length ratios between the models and their natural prototype (see Table 2 for different crustal thickness). This time window suggests a rapid rifting and rotation of the high-angle fault to a low-angle detachment. Lack of syn-rift sediments at the ocean–continent transition (Wilson and Manatschal, 1999) supports model conclusion of fast rifting.

4.1. Block rotation

During extension of models 1– 3 and 6, where the upper

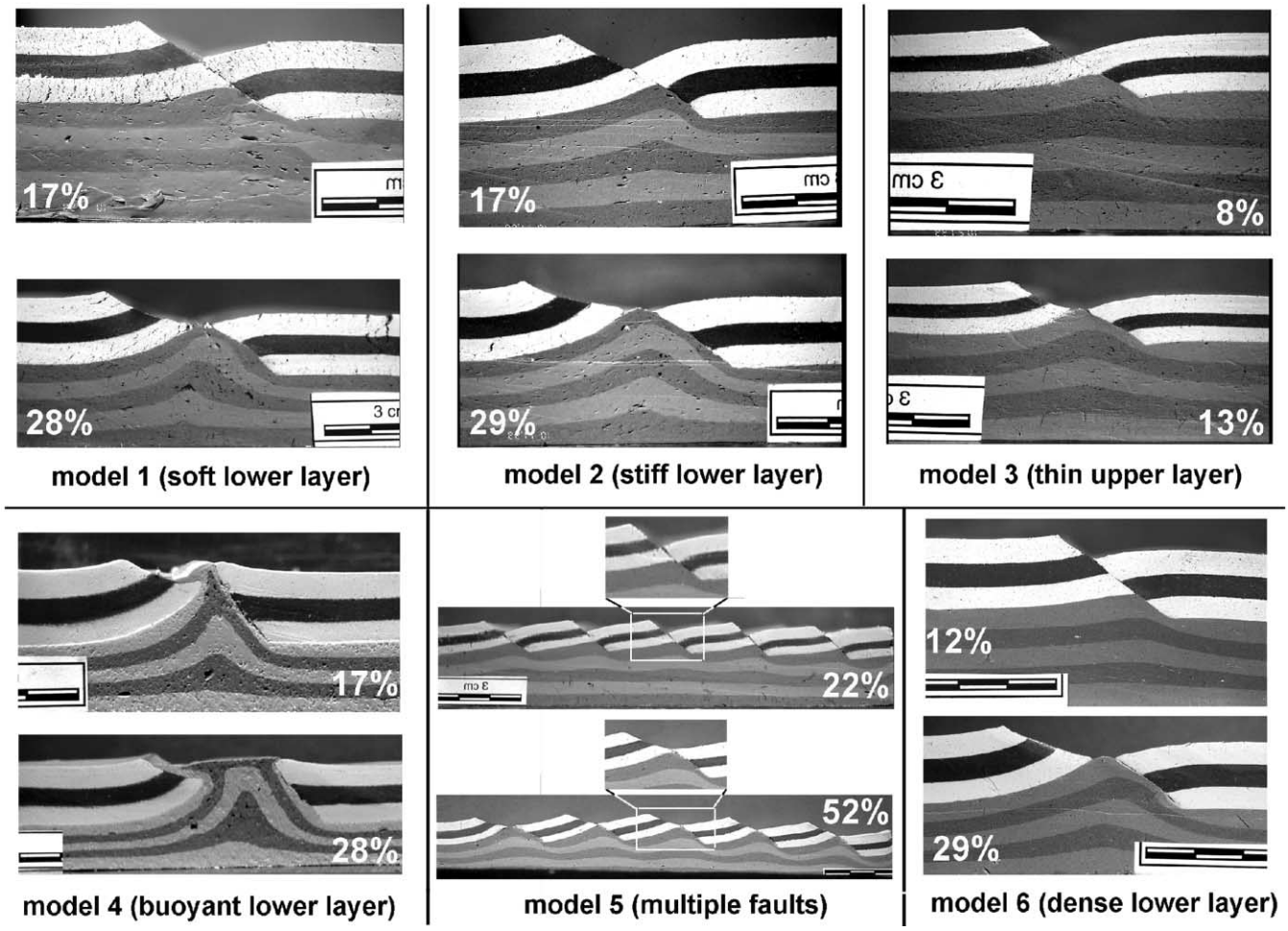

Fig. 3. Profiles of models 1–6 at different percentage of bulk extension. In models 1– 3, and 6, the hanging wall forms a rollover anticline during extension of the models. Note that the rollover becomes less prominent after separation of the two blocks. This structure does not form in models 4 and 5. In model 4, the rollover does not form because of the buoyant rise of the lower layer. In model 5, the rollover does not form because the blocks do not deform internally but rotate as a relatively rigid body. Note that in model 5, extension is distributed over a wide area involving five faults, four of which remain close to planar even after separation of the blocks. Note also that in all models the asymmetric flow of the ductile lower material before separation of the two blocks becomes more asymmetric after separation. The bottom layer of the footwall is thinned by the drag of the upwelling material.

layer is cut by only one prescribed *fault* and rests on a lower layer of equal or greater density (Figs. 1 and 3), both the hanging wall and footwall blocks underwent internal deformation. The hanging wall developed a rollover anticline which became more open after separation of the two blocks and the isostatic upwelling of the lower layer to fill the gap (Fig. 3). In these models, the footwall block underwent a gradual upward bending (rollunder) that culminated during the separation of the two blocks (Fig. 3). Egan (1992) used two-dimensional models to predict footwall uplift between a few tens of meters to 1.5 km, which can be closely correlated with the amount of footwall uplift deduced from the geological record.

Deformation of the hanging wall and footwall blocks in model 5 was different from models 1–3 and 6. During extension of model 5, where the upper layer was cut by five prescribed *faults* (Figs. 1 and 3), rather than deforming internally, individual blocks rotated as relatively rigid bodies without much internal deformation. In this model, the weak rollover anticlines that formed in the hanging walls of the faults disappeared after the blocks separated during extension (Fig. 3). In general, the distributed extension along the normal faults in model 5 promoted rotation of the faulted blocks rather than their deformation. As a result, the fault surfaces remained more planar (than in the other models) as they rotated to shallower angles without becoming horizontal (Fig. 3). Only the footwall block that was attached to the endwall of the model was not able to rotate in a rigid-body fashion. Hence, it deformed internally, resulting in bending of the fault surface from a planar to a listric geometry (Fig. 3). In this model, this was the only fault which deformed to a sub-horizontal detachment fault. Applied to nature, these results suggest that intrabasinal faults are less likely to become listric since the blocks containing them rotate instead of being internally deformed. As a result, the rotation of blocks preserve faults as planar.

Marginal faults, on the other hand, are more likely to deform to listric geometry since the blocks containing them are attached and cannot rotate as rigid bodies, but deform internally instead.

Deformation in model 4, which had a buoyant lower layer, was dominated by the upwelling buoyant material that prevented the formation of a rollover in the hanging wall block and promoted rotation and deformation of the footwall block internally at less bulk extension (17%) than in the models with a denser lower layer material. In the model with a less buoyant lower layer (model 4), and in the model with a thinner semi-brittle upper layer (model 3), the fault became listric at half the amount of bulk extension (13–17% compared with about 30% for models with a denser ductile layer or models with a thicker semi-brittle layer).

In general, the deformation of the hanging wall and footwall blocks was different. Rollover of the hanging wall, which was at its maximum at early stages of extension, decreased to become gentler at later stages of extension (Fig. 3). The deformation of the footwall, on the other hand, was progressive; the rollunder of the footwall block increased with accumulative extension, reaching its culmination during the separation of the two blocks (Fig. 3).

It is worth pointing out that the hanging wall deforms independently of the footwall. During the listric rotation of the *fault* in the footwall, the hanging wall part of the fault becomes anti-listric. This feature is most visible in models 1–3 and 6, where the hanging wall is distorted to anti-listric during the formation of the rollover. This anti-listric geometry was less profound during the separation of the blocks (Fig. 3).

4.2. Localised extension

In all models (1–4 and 6), where the upper layer was cut by only one prescribed *fault*, extension was localised along the pre-existing cut in the upper layer. Here, the fault surface was deformed to listric geometry and produced low-angle detachments during later stages of extension. In the model with a thin upper layer (6 mm; model 3), the deformation from a high-angle fault to low-angle detachment was reached after less than 10% extension. By comparison, models with a thicker upper layer (12 mm; models 1 and 2) reached the same stage after (30%) extension. However, in model 4, where the upper layer was 12 mm thick and rested on a buoyant mantle, the fault became listric and deformed to a low-angle detachment after a significantly lower amount of bulk extension (17%). This is attributed to early diapiric rise of the buoyant lower layer that deformed both portions of the fault (Fig. 3). In model 5 with several prescribed cuts, upwelling of the lower ductile layer is distributed over a wide area, whereas in the other four models with one prescribed cut, this upwelling is concentrated along a narrow zone between the two separating blocks (Fig. 3). In this sense, the results of our models are consistent with Boutilier and Keen's (1994) numerical models which show that in the presence of two prescribed cuts at a far distance (110 km) from each other, the faults remain planar during extension and the mantle upwelling will be distributed rather than localised.

In model 6, where the lower layer was denser, a similar deformation style to those in models 1–3, where the lower layer had an equal density to that of the upper layer, was observed. This indicates that the isostasic upwelling of the lower layer occurs in all models irrespective of its density and that the density of the lower layer is less significant in influencing the deformation style of the models.

Manatschal and Froitzheim (1999) argue that evidence from the Iberian ocean–continent transition is indicative of a transition from high-angle normal faults to low-angle detachment faults occurring late in the exhumation process, potentially following a localisation of deformation. In models 1–3, which contain a lower layer of equal density as the upper layer and in model 6 with a denser lower layer, flattening of the high-angle faults took place late in the exhumation process. Previous models (Brun et al., 1994) argue that detachment faulting in the upper layer results due to the presence of a *weak heterogeneity* in the lower layer. We argue that localisation of extension by any mechanism whatsoever (including the presence of a *weak heterogeneity* in the lower layer) will result in detachment faulting, i.e. localisation of extension and not presence of a *weak heterogeneity*, is the critical prerequisite for detachment faulting. We do accept, however, that presence of a *weak heterogeneity* may be instrumental in localising extension both in the same core complex terrains and the same OCT zones. In core complex terrains, this *weak heterogeneity* might be a partially molten zone and at OCT zones, serpentinized mantle. The first high-angle normal faults that penetrated the crust during extension may have provided suitable conduits for the required downflow of water to the mantle. Serpentinization will have therefore occurred at the tip of these faults, creating the ideal conditions for localised extension within a narrow area of the crust. Continued extension and subsequent mantle upwelling would therefore have been restricted to the close vicinity of these faults. We argue that localised extension promotes localised upwelling, which in turn accentuates block rotation and bending of high-angle normal faults to become listric. Govers and Wortel (1993) used finite element models to show that the development of detachment faults is likely in the transition zone of the continental lithosphere where normal shearing occurs along the dipping zone of localised deformation in the lower crust.

5. Conclusions

Scaled centrifuge models consisting of a semi-brittle layer resting on a ductile layer suggest that:

1. Localised extension promotes formation of low-angle detachment faults from deformed high-angle normal faults. The viscosity and density of any underlying layer contribute to enhancing localisation of deformation.
2. When extension is distributed among several faults, the faults stay planar because of block rotation even after a significant amount of extension.
3. Coupling of deformation between the faulted layer and the underlying ductile layer is essential for the formation of low-angle detachments from high-angle normal faults.
4. Internal deformation rather than rotation of faulted blocks is responsible for the formation of low-angle detachments from high-angle faults.
5. The only situation where localisation of extension will not result in detachment faulting is where the upper and lower layers are totally decoupled.

Acknowledgements

Thanks are due to John Dixon and Michael Wells for their thorough and constructive reviews, and Chris Talbot for commenting on the manuscript. HAK was funded by the Swedish Natural Sciences Research Council (NFR). ADLS was funded by a European Commission Training and Mobility of researchers (Marie Curie) fellowship.

References

Angelier, J., Colletta, B., 1983. Tension fractures and extensional tectonics. Nature 301, 49–51.

Axen, G.J., Fletcher, J.M., Cowgill, E., Murphy, M., Kapp, P., MacMillan, I., Ramos-Velasquez, E., Aranda-Gomes, J., 1999. Range-front fault scarps of the Sierra El Mayor, Baja California: formed above an active low-angle normal fault?. Geology 27, 247–250.

Bartley, J.M., Wernicke, B.P., 1984. Hydrothermal systems and tertiary low-angle normal faulting in the western United States. Geology 13, 562–564.

Boutilier, R.R., Keen, C.E., 1994. Geodynamic models of fault-controlled extension. Tectonics 13, 439–454.

Brun, J-P., Sokoutis, D., Van Den Driessche, J., 1994. Analogue modeling of detachment fault systems and core complexes. Geology 22, 319–322.

Buck, W.R., Martinez, F., Steckler, M.S., Cochran, J.R., 1988. Thermal consequences of lithospheric extension: pure and simple. Tectonics 7 (2), 213–234.

Buck, W.R., 1988. Flexural rotation of normal faults. Tectonics 7 (5), 959–973.

Burchfiel, B.C., Zhiliang, C., Hodges, K.V., Yuping, L., Royden, L.H., Changrong, D., Jiene, X., 1992. The south Tebetan detachment system, Himalayan orogen: Extension contemporaneous with and parallel to shortening in a collisional mountain belt. Geol. Soc. Am. Special Paper 269, p. 41.

Davis, G.H., 1983. Shear-zone model for the origin of metamorphic core complexes. Geology 11, 425–440.

Davis, G.A., Andersson, J.L., Frost, E.G., Shackelford, T.J., 1980. Mylonitizationand detachment faulting in the WippleBuckskin-Rawhide Mountains terrane, southeastern California and western Arizona. Geol. Soc. Am. Mem. 153, 79–129.

Den Driessche, V., Brun, J-P., 1992. Tectonic evolution of the Montagne Noire (French Massive Central): a model of an extensional gniess dome. Geodinamica Acta 5, 85–101.

Dixon, J.M., Summers, J.M., 1985. Recent developments in centrifuge modelling of tectonic processes: equipment, model construction techniques and rheology of model materials. J. Struct. Geol. 7, 83–102.

Egan, S.S., 1992. The flextural isostatic response of the lithosphere to extensional tectonics. Tectonophysics 202, 291–308.

Govers, R., Wortel, M.J.R., 1993. Initiation of asymmetric extension in continental lithosphere. Tectonophysics 223, 75–96.

Harry, D.L., Bowling, J.C., 1999. Dynamic models of non-volcanic rifting and evolution of the Iberia passive continental margin. Tectonic Studies Group Abstr., 22.

Koyi, H., 1988. Experimental modeling of role of gravity and lateral shortening in Zagros Mountain Belt. Am. Assoc. Petrol. Geol. Bull. 72, 1381–1394.

Koyi, H., 1991. Gravity overturns, extension, and basement fault activation. J. Pet. Geol. 14, 117–142.

Lister, G.S., Davis, G.A., 1989. The origin of metamorphic core complexes and detachments faults formed during tertiary continental extension in the northern Colorado River region, USA. J. Struct. Geol. 11, 65–94.

Lister, G.S., Etheridge, M.A., Symonds, P.A., 1991. Detachment models for the formation of passive continental margins. Tectonics 10, 1038–1064.

Manatschal, G. and Froitzheim, N., 1999. Detachment faulting along non-volcanic margins: insights from the Iberia Abyssal Plain, in: Non-volcanic Rifting of Continental Margins: A Comparison of Evidence from Land and Sea, Abstracts of Talks and Posters, 31.

Miller, E.L., Gans, B.P., Garling, J., 1983. The Snake river decollement: an exhumed mid-tertiary brittle-ductile transition. Tectonics 2, 239–263.

Ramberg, H., 1981. Gravity, Deformation and the Earth's Crust: 2. Academic Press, London, p. 452.

Sawyer, D.S., 1994. The case for slow-spreading oceanic crust landward of the predotitie ridge in the Iberia abyssal plain. EOS 75, 616.

Selverstone, J., 1988. Evidence for east–west crustal extension in the eastern Alps: implications for the unroofing history of the Tauern Window. Tectonics 7 (1), 87–105.

Wernicke, B., 1981. Low-angle normal faults in the Basin and Range Province: nappe tectonics in an extending orogen. Nature 291, 645–648.

Wernicke, B., 1985. Uniform-sense normal simple shear of the continental lithosphere . Canadian Journal of Earth Sciences 22 (1), 108–125.

Wernicke, B., Axen, G.J., 1988. On the role of isostasy in the evolution of normal fault systems. Geology 16 (9), 848–851.

Wilson, R.C.L., Manatschal, G., 1999. The timing, duration and location of rifting along cold passive margins: evidence from the Mesozoic of the eastern Atlantic and the Alps. Tectonic Studies Group Abstr., 54.